Polymer Films on Electrodes

XXVII. Electrochemical and Ellipsometric Measurements of a Viologen-Siloxane Polymer Film: Deposition, Solvent Swelling, Oxidation-State-Dependent Thickness, and Charge Transport

Larry J. Kepley* and Allen J. Bard**

Department of Chemistry and Biochemistry, The University of Texas at Austin, Austin, Texas 78712, USA

ABSTRACT

In situ ellipsometry was used to study the electrodeposition of the viologen-based redox polymer formed by electroreduction of *N,N'*-bis[-3-(trimethoxysilyl)propyl]-4,4'-bipyridinium dichloride (**I**) at Pt electrodes. The importance of dimerization of the 1+ species in the film was demonstrated by comparing voltammetric results for thin films of the polymer with equations derived for the current, peak potential, and limiting shape of thin layer, linear sweep voltammograms for a kinetically reversible couple, where one form of the couple undergoes fast reversible dimerization. The complex refractive index and viologen concentration for solvent swollen films were determined for the 2+ and 1+ states of the viologen groups during film growth. The polymer deposited isotropically to thicknesses of ≤400 nm (2+ state). High quality films for ellipsometric measurements were also formed by spin-coating the electrode with ethanolic solutions of **I**. The film optical constants, degree of film swelling by solvent sorption, and changes in swelling associated with reduction in blank electrolyte solution were determined from least squares analysis of data for multiple angles of incidence, without resorting to auxiliary measurements. Reduction caused film shrinkage of about 25%. Modeling of transient ellipsometric data for large potential steps was used to test the theory that electron transport represents a diffusion process. Theoretical curves were calculated by treating the film as a system of stratified layers whose optical constants were given by effective medium theory using the refractive indexes of completely reduced and oxidized films and simulated thin layer conversion profiles (*i.e.*, gradients) for diffusional transport. During film reduction, hopping of electrons (between 1+ and 2+ centers) effectively followed a diffusion model, with reduction proceeding outward from the electrode/film interface. Film oxidation back to the 2+ state was slower and required film reswelling, which lagged the extent of oxidation during both fast and slow conversions (*i.e.*, during potential steps and sweeps). Ellipsometric data provided the first direct evidence that film expansion driven by a redox process can impede charge transport.

Research of polymer modified electrodes (PMEs) is now a fairly mature area.[1,2] Electron transport in polymers containing bound redox sites (redox polymers) occurs by electron hopping between neighboring redox centers.[3] In the simplest case, where the negligible resistive potential drop or phase changes occur in the film, electron transport can be represented as a diffusion process with an effective diffusion coefficient (D_e).[4] However, electron transport during electrochemical conversion of redox polymers can be influenced by coupled processes, such as counterion migration or changes in levels of film swelling by electrolyte solution, to yield an overall observed charge-transport rate (D_{ct}). Film swelling by solution is important,[5-9] because electron transfer and ion transport both require local chain motion and conformational freedom. Segmental chain motion controls the collision frequency of redox centers[10,11] and also creates free volume necessary for ion mobility.[12] The degree of swelling can vary from about 15 to 180% for nonpolar aprotic polymers[13-16] to as much as 100-fold for a protonated polar polymer.[17]

In studies of PMEs the question typically arises: does $D_{ct} = D_e$, or does D_{ct} represent limitations from coupled processes? The presence of counterion or film swelling limitations in redox polymers is not easily discernible from voltammetric measurements alone. PMEs suspected of being counterion-transport limited can also give linear chronoamperometric and chronocoulometric plots indicative of diffusion-limited transport.[18,19] Electrolyte dependencies can suggest the presence of ion transport limitations, but the nature of the electrolyte solution can also affect intrinsic electron hopping rates by its influence on chain packing and dynamics.[20] Furthermore, D_{ct} can be larger than D_e due to field-enhanced electron hopping (*i.e.*, electron migration),[21] if a significant electric field develops across the film as a result of poor ion mobility,[22] which again raises the possibility of nondiffusional electron transport.

We discuss here simultaneous voltammetric and ellipsometric measurements of film swelling and conversion of the siloxane-paraquat redox polymer ($PQ^{2+/+}$) formed by hydrolysis and condensation of *N,N'*-bis[-3-(trimethoxysilyl)propyl]-4,4'-bipyridinium dichloride, **I**.[23,24] We

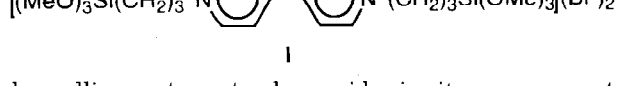

I

show ellipsometry not only provides *in situ* measurements of film thickness (d) as a function of oxidation state, which can give information about the effects of changes in film swelling on D_{ct}, but that its sensitivity to redox conversion gradients can be used to verify optically that diffusional transport prevailed. Ellipsometry has been used previously to determine whether conversion proceeded either outward from the electrode/film interface or inward from the film/solution interface during electrochemical interconversion of metal oxides,[25] conducting polymers,[26-28] and polythionine.[29] The work presented here is the first ellipsometric study of a highly swollen redox polymer.

$PQ^{2+/+}$ was chosen as a good model system for the following reasons: (*i*) its chemical stability and intense coloration upon reduction allowed the precision and sensitivity necessary to determine the conversion gradient. (*ii*) Film conversion rates for this polymer yield some of the largest D_{ct} values yet reported, making the level of film swelling and the *in situ* redox site concentration for this system especially interesting. D_{ct} cannot be determined without knowledge of the solvent-swollen film thickness. (*iii*) $PQ^{2+/+}$ films display almost ideal thin-layer behavior and the viologen centers form dimers when reduced (Eq. 1 and 2), so $PQ^{2+/+}$

$$PQ^{2+} + e^- \rightleftharpoons PQ^+ \qquad [1]$$

$$2PQ^+ \underset{k_b}{\overset{k_f}{\rightleftharpoons}} (PQ^+)_2 \qquad [2]$$

films were suitable for testing the theory for thin-layer voltammetry of reversible electron transfer with following dimerization. Reversible dimerization has been seen for other polymer-bound organic redox groups, including 10-methylphenothiazine (PTZ),[30] tetrathiafulvalene (TTF),[3b] and tetracyanoquinodimethane (TCNQ).[31] Theory has been presented for the case of a following irreversible dimeriza-

* Electrochemical Society Student Member.
** Electrochemical Society Fellow.

Table I. PQ^{2+} film thicknesses and optical constants for various ambient phases.

Film	Ambient phase	n_1	k	d(nm)	$C^*_{PQ^{2+}}$ (M)
A[a]	N_2 gas	1.56 ± 0.12	0.04 ± 0.04	80 ± 10	1.9 ± 0.2
	H_2O vapor (*ca.* 100% humidity)	1.41 ± 0.005	0.005 ± 0.005	189 ± 5	0.80 ± 0.03
	MeCN-vapor	1.55 ± 0.01	0.005 ± 0.005	125 ± 5	1.22 ± 0.06
	1.0 M KCl soln-vapor	1.47 ± 0.01	0.005 ± 0.005	149 ± 5	1.02 ± 0.05
	1.0 M KCl soln	1.46 ± 0.01	0.005 ± 0.005	145 ± 5	1.05 ± 0.05
B[b]	N_2 gas	1.77 ± 0.02	0.005 ± 0.005	88 ± 3	—
	H_2O vapor	1.50 ± 0.02	0.001 ± 0.002	190 ± 3	—
	1.0 M KCl	1.49 ± 0.02	0.005 ± 0.005	178 ± 3	1.0 ± 0.05
C[c]	N_2 gas	1.531 ± 0.005	0.007 ± 0.0004	251 ± 1	—
	1.0 M KCl	1.451 ± 0.006	0.005 ± 0.004	464 ± 10	1.03 ± 0.05

[a] $\Gamma = 1.52\ (\pm 0.05) \times 10^{-8}$ mol/cm^2, from area of first CV in 1.0 M KCl.
$\Gamma = 1.6\ (\pm 0.2) \times 10^{-8}$ mol/cm^2, from area of last deposition CV.
$\tilde{N}_{Pt} = 1.80 - 4.60\hat{\imath}$, $\tilde{N}_{soln} = 1.341 - 0\hat{\imath}$.
[b] $\tilde{N}_{Pt} = 1.85 - 4.25\hat{\imath}$; baked in vacuum oven at 0.01 Torr, 60°C.
[c] $\tilde{N}_{Pt} = 1.86 - 4.15\hat{\imath}$; spin coated from EtOH.

tion[32] but not for a reversible system. (*iv*) The PQ system, like some other redox polymers (plasma-polymerized vinylferrocene,[7,33] PTZ, [30] and TTF [3b,5]), shows unequal forward and reverse conversion rates, possibly as a consequence of changes in film swelling, so it is a good system for testing the importance of changes in swelling on D_{ct}.

Film swelling driven by solvent and ion uptake can affect the electrochemical reaction thermodynamics, when the mechanical energy for film expansion (*i.e.*, PV work) is coupled to the energetics of the electrochemical reaction.[34] Changes in d *vs.* oxidation state have been measured by profilometry of dry TTF-functionalized polystyrene films,[5] *in situ* stylus response of a benzylviologen-siloxane polymer,[13] and ellipsometry of polyvinylferrocene[35] and polythionine[16] films; all showed about a 15% increase on conversion to their more charged state. We expect that coupling of the rate of film expansion to the rate of conversion should occur, and such kinetic coupling might contribute to the large differences reported for D_{ct} based on steady-state *vs.* transient methods.[36-38] We monitored $PQ^{2+/+}$ film conversion ellipsometrically as a function of time during potential steps and sweeps to see if slow film swelling was associated with the smaller D_{ct} observed for oxidation.

Experimental

Chemicals.—*N,N'*-bis [-3-(trimethoxysilyl)propyl] 4,4'-bipyridinium dibromide was either prepared in this laboratory by J. G. Gaudiello following published procedures[23] or received as a gift from M. Wrighton. Water was purified with a Milli-Q ion exchange system (Millipore Corporation) equipped with an Organex-Q cartridge and a 0.22 μm final filter. Acetonitrile (MCB Reagents) was vacuum distilled twice from P_2O_5 and loaded into the cell in a dry box. All other chemicals were reagent grade and used as received.

Electrodes.—The reference electrode was a standard NaCl calomel electrode (SSCE); a large Pt screen served as the counterelectrode. A Pt working electrode (area = 0.164 cm^2) was made by brazing a 0.5 mm thick Pt disk (Johnson-Matthey/AESAR, 99.99%) to the end of a brass rod with Ag-based solder before turning down the end in a lathe to 0.180 in. diam. It was then butted against a glass rod of slightly smaller diameter, encased in heat-shrinkable fluorinated ethylene-propylene (FEP) Teflon tubing, and pressed into a tetrafluorethylene (TFE) Teflon cylinder undersized by about 0.025 in. Compression from the undersized TFE Teflon shroud sealed the inner tubing against the Pt/brass rod. The shroud was turned down to 1.000 in. diam and faced-off along with the Pt surface to achieve coplanarity. Successive polishing with 6, 1, and 0.25 μm diamond paste slurries on nylon pads (Buehler, Ltd.) gave a mirror finish. A gold-plated pin connector soldered to the brass rod provided electrical contact. Before each experiment, the electrode was repolished with 1 or 25 μm paste, sonicated in ethanol, cleaned electrochemically by cycling between the potentials for hydrogen and oxygen evolution in degassed 0.5 M H_2SO_4, removed at 1.1 V, and rinsed with water.

The ellipsometrically measured complex refractive index ($\tilde{N} = n - k\hat{\imath}$) of the Pt surface varied slightly between experiments because of differences in alignment and the final polishing step. Polishing with 0.25 μm paste, which did not lather well and gave the surface an anomalously high extinction coefficient (k = 4.65) and a slightly angle-dependent refractive index, was used in the surface preparation initially. This was discontinued because a 1.0 μm polish gave more reproducible measurements of $\tilde{N}_{Pt}$ (about 1.86 − 4.20$\hat{\imath}$ in air and in solution, λ = 632.8 nm) which were consistent with reported values for Pt.[39-42]

Film preparation.—Film-coated electrodes were prepared either by electroprecipitation of **I** from 0.2 M K_2HPO_4/0.1 M KCl solutions (pH 8.9) or by spin coating the surface with a EtOH solution of **I** under a dry N_2 blanket. Spin-cast films are noted as such in the table footnotes. Aqueous solutions of **I** were prepared by slowly adding it to water with rapid mixing before adding buffer and adjusting pH, because organotrialkoxysilanes hydrolyze more rapidly in alkaline solution to silane triols, which form cross-linked, colloidal, insoluble polysiloxanols.[43] Electrodeposited films were formed from filtered, *ca.* 3 mM solutions of **I** in N_2-purged single compartment cells by repeatedly cycling E between 0.0 and −0.78 V at sweep rates (v) of 20 to 100 mV/s. When coated electrodes were studied in a blank 1.0 M KCl solution, they were first rinsed with water and dried briefly in a N_2 stream. $\tilde{N}_{Pt}$ is given for each experiment. The uncertainty in $\tilde{N}_{Pt}$ caused by the presence of a native oxide layer changes in interfacial structure as a function of potential, and variations in surface polishing (about 3% of n and k) had a negligible effect on estimates of $\tilde{N}$ and d for the film, because the films were thick compared to interfacial layers. Changing n_{Pt} or k_{Pt} by 5% affected estimates of n, k, and d for films by only 1 to 2%. Following a procedure similar to that used by Willman and Murray to prepare benzylviologen-silane films,[44] we prepared spin-cast films by applying a drop of monomer solution (about 5 mg of **I** per 10 drops of EtOH) while spinning the electrode at 7000 rpm in a photoresist spinner (Model EC101, Headway Research, Inc., Garland, TX). The casting solution was prepared in air, centrifuged for 1 min (Eppendorf Model 5412), and immediately pipetted onto the electrode under N_2 gas. New films kept under flowing N_2 gas shrank 3% over 12 h. They were cycled twice between dry N_2 and air atmospheres to promote hydrolysis, coupling, and cross-linking of the silane groups. Exposure to air caused reversible film swelling of about 140%. Except for film B in Table I, films were not baked, because baking

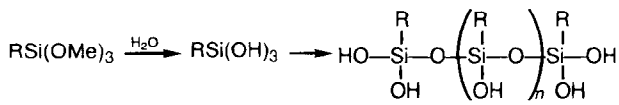

Scheme I

did not improve their stability or affect their properties noticeably.

Optical cell and instrumentation.—A custom Teflon cell described previously[45] with cylindrical windows for incidence angles (Ω) from 55 to 80° *vs.* surface normal was used for all ellipsometry measurements. The reference electrode was mounted with a Swagelok fitting. An auxiliary solution compartment attached to the top port of the cell housed the counterelectrode and was vigorously purged with N_2 without introducing bubbles into the optical path. During vapor swelling measurements, 100% relative humidity was achieved by recirculating the cell atmosphere through a water bubbler with a peristaltic pump.

Ellipsometric measurements were made with a Rudolph Research Model 2437 ellipsometer equipped with a Model RR2000FT rotating analyzer detector, using 632.8 nm light from a 5 mW He-Ne laser. Fast data acquisition rates (27 Ψ-Δ points per second; 37.0 ms/point with an 18.52 ms observation period) and least squares fitting of multiple-thickness data were achieved using software written on a Hewlett-Packard Model 9816S computer. Multiple angle of incidence (MAI) data was fit using the SYSNLIN regression analysis software from the Statistical Analysis Software Institute on an IBM 3081 computer. Electrochemistry was performed using a EG&G Princeton Applied Research Model 175 potential programmer, Model 173 potentiostat, and Model 179 digital coulometer; Hewlett-Packard Model 7045B and Houston Instruments Model 2000 X-Y recorders; and a Norland Model 3001 digital oscilloscope.

Results

Monomer electrodeposition.—In situ ellipsometry was used to monitor film growth during reductive precipitation of **I** from solution. While continuously cycling between reduction and reoxidation of the viologen sites, the ellipsometric angles (Ψ and Δ) were recorded for each $PQ^{2+/+}$ state during film growth (Fig. 1). Data curves A and B were obtained by recording one Ψ-Δ point at each sweep limit of each deposition cycle: $E = -0.75$ and 0.0 V, respectively. Also shown in Fig. 1 are data for the subsequent film swelling (curve C) and dissolution (curve D) that occurred while holding the film in the PQ^{2+} state.

The complex refractive index ($\tilde{N} = n - k\hat{i}$) of the film for each oxidation state was determined by least squares analysis of each data curve, using the overall reflection coefficients for a single, isotropic layer between semi-infinite phases[46] and measured $\tilde{N}$ values for the bare Pt electrode and the solution ($\tilde{N}_{Pt} = 1.81 - 4.65\hat{i}$ and $\tilde{N}_{soln} = 1.337 - 0\hat{i}$).

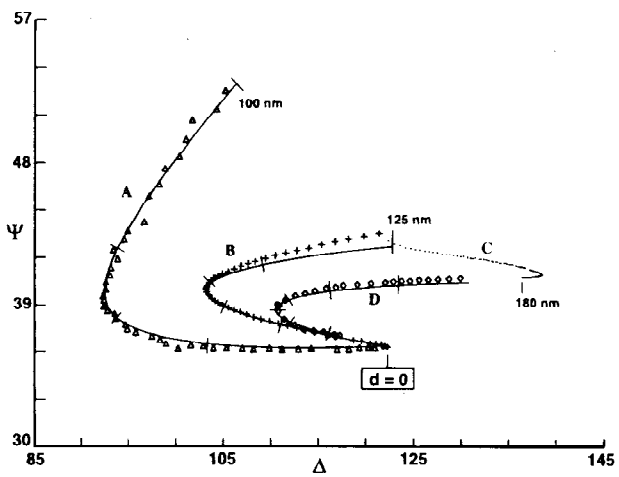

Fig. 1. Experimental ellipsometric data (points) and calculated (curves) for the (A) 1+ and (B) 2+ states of a $PQ^{2+/+}$ film during growth (E swept continuously from 0.0 to −0.75 V, v = 100 mV/s), (C) subsequent film swelling (E = 0 V) and (D) dissolution. Film $\tilde{N}$ for calculated curves (A) 1.660 − 0.11$\hat{i}$, (B) 1.515 − 0$\hat{i}$, and (D) 1.425 − 0$\hat{i}$. Tick marks indicate 25 nm increments in thickness. θ = 67°, $\tilde{N}_{Pt}$ = 1.81 − 4.65$\hat{i}$.

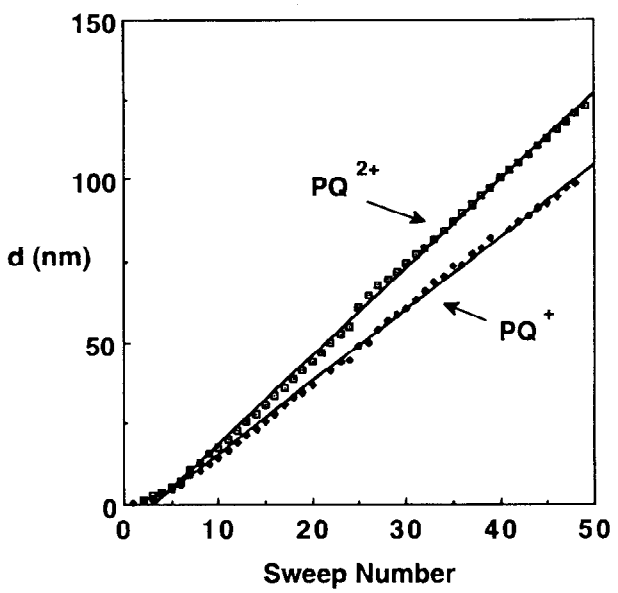

Fig. 2. Calculated film thicknesses for the data in Fig. 1 *vs.* number of reductive sweeps. Curve fitting gave: $d_{PQ^{2+}} = 2.7 \cdot$ (sweep no.) − 8.4, $d_{PQ^{+}} = 2.2 \cdot$ (sweep no.) − 6.4; $d_{PQ^{+}}/d_{PQ^{2+}} = 77\%$ from ratio of slopes.

Best fits ($\tilde{N}_{PQ^{+}} = 1.660 - 0.110\hat{i}$ and $\tilde{N}_{PQ^{2+}} = 1.515 - 0\hat{i}$) were obtained by searching a grid of n and k values for the lowest total error sum, where d and the error sum for each Ψ-Δ point ($[\Delta - \Delta_{calc.}]^2 + [\Psi - \Psi_{calc.}]^2$) was found by a line search of d for each set of n and k values. Best fit curves generated by incrementing the film thickness in the reflection equations are shown in Fig. 1 as solid curves over the data points. $k_{PQ^{2+}} = 0$ not only gave the best fits of PQ^{2+} data but also was required for self-consistent fits in which d increased smoothly for points in the bend of the Ψ-Δ plots. The slight deviation of the calculated curve from the data curve for the 2+ state at $d > 75$ nm reflects a small artificial increase in $k_{PQ^{2+}}$ due to incomplete oxidation as the film grew thicker. The agreement of the experimental and theoretical Ψ-Δ data in Fig. 1 and of that (not shown) for thicker films ($d_{PQ^{2+}} > 400$ nm) shows that films deposited isotropically with a constant refractive index for each state. No asymmetric behavior representative of anisotropy of the kind reported for Langmuir-Blodgett films[46b] was observed in Ψ-Δ plots for the transparent (2+) state, even when the plots traversed a complete revolution (*i.e.*, a 2π change in the film phase thickness).

Scattering by surface roughness was not a problem during potential-sweep depositions, when freshly prepared solutions were used. However, potentiostatic reduction at −0.74 V produced a rough film that scattered the light beam completely when d reached about 70 nm. Varying the sweep rate (v = 20 to 100 mV/s) had no effect on film quality, because there was ample time during each cycle for the PQ^{2+} film to swell and restructure to give a smooth film. Doubling v required about twice as many deposition cycles to reach the same film thickness.

Plots of d *vs.* deposition-cycle number (Fig. 2) were linear after a short induction period, and the ratio of their slopes shows that reduction caused film shrinkage of 33%. Viologen concentrations (C^*) for each state were calculated from the charge under voltammetric peaks and corresponding film thicknesses: $C^*_{PQ^{2+}} = 1.4 \pm 0.1$ M and $C^*_{PQ^{+}} = 1.8 \pm 0.1$ M. The large error estimates stem from the difficulty of measuring the peak areas for surface-confined groups exclusive of areas for **I** in solution. Peak areas for forward and reverse sweeps were equal, so the change in C^* represents film shrinkage only.

With reference to Fig. 1, ellipsometric data recorded just after the last deposition cycle, while holding E at 0.0 V, show that undried films swelled extensively (curve C) before slowly dissolving back into solution (curve D). The

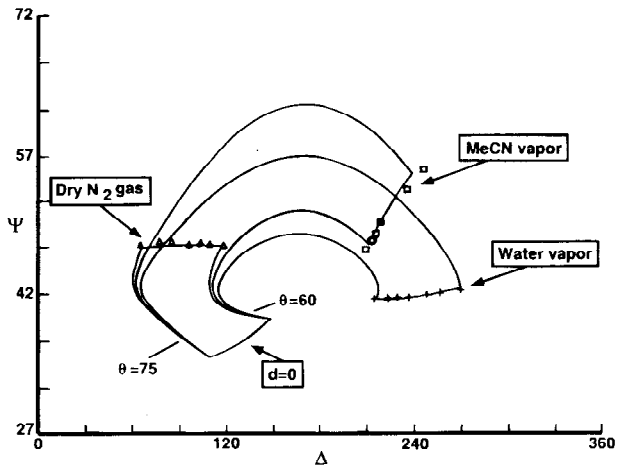

Fig. 3. MAI data sets (points, θ = 60 to 75°) for PQ^{2+} film as a function of bathing gas and least squares fits: $\tilde{N}$ = 1.667 − 0i, d = 71 nm for dry N_2; $\tilde{N}$ = 1.547 − 0i, d = 125 nm for MeCN vapor; and $\tilde{N}$ = 1.410 − 0i, d = 189 nm for water vapor. Also shown are calculated growth curves for θ = 60 and 75° and the MAI curve for bare Pt ($\tilde{N}$ = 1.8 − 4.6i).

increase in Δ and drop in Ψ in curve C, which began within seconds of stopping E at 0 V and occurred over the 20 min period, represent an increase in d and a drop in $n_{PQ^{2+}}$. Swelling was rapid at first, about half complete in 3 min, and continued for 17 min until dissolution became the dominant process, causing the sharp bend in curve C. A comparison of the least squares fit of multiple angles of incidence (MAI) data recorded in between curves C and D ($n_{PQ^{2+}}$ = 1.440 ± 0.005, $k_{PQ^{2+}}$ = 0.0 ± 0.005, and $d_{PQ^{2+}}$ = 180 ± 5 nm) to the values for the film at the end of the deposition ($n_{PQ^{2+}}$ = 1.515 ± 0.005, $k_{PQ^{2+}}$ = 0.00 ± 0.005, and $d_{PQ^{2+}}$ = 125 ± 5 nm) confirmed that the film became considerably more swollen when not cycled between states. Film dissolution (curve D) was much slower than swelling, only about half complete in 1.5 h, and required 24 h to almost finish (*i.e.*, d = 20 nm). The good fit of the data in curve D by the calculated curve for $n_{PQ^{2+}}$ = 1.425 shows that the film refractive index remained fairly constant during dissolution after dropping initially from 1.44 in 1.5 h. The constancy of $n_{PQ^{2+}}$ suggests that dissolution progressed inward from the film/solution interface, etching the film away without leaching material from within to give increased porosity and associated decrease in $n_{PQ^{2+}}$.

Solvent swelling and dimerization of PQ^+ centers.—Very stable films and accurate estimates of *in situ* thicknesses and optical constants are required to model transient ellipsometric data meaningfully. Regression analysis of MAI data, which has not been used previously for polymer films, was an excellent way to determine the optical constants and thickness of preformed films. It was particularly convenient for measuring solvent swelling of dried films. Typical MAI data sets for a PQ^{2+} film exposed to different bathing gases, dry N_2 gas, acetonitrile vapor, and water vapor, are shown in Fig. 3, along with calculated MAI plots (best fits) drawn at the terminal ends of theoretical film-growth (multiple d) plots for the high and low θ of the data set and the corresponding film $\tilde{N}$ values. The film growth curves are shown to illustrate the phase thickness of each film, that is, the location of the data along the periodic Ψ-Δ plots for constant $\tilde{N}$, which is useful in visualizing the dependencies of Ψ and Δ on n, k, and d. Table I summarizes results for a variety of ambient phases. Good estimates of n, k, and d were obtained except when Δ fell near its inflection point (*i.e.*, its minima) in film growth curves for small k (*i.e.*, $k \leq 0.1$), which occurs at about d = 70 to 90 nm for a range in n typical of polymers (n = 1.7 to 1.4);[47] details are given elsewhere.[45b] In this parameter subspace the dependencies of Ψ on n and k are small and correlated throughout the useful range of θ, making fits somewhat insensitive to k in the range 0 to 0.1. However, the uncertainty in k and consequently in n had only a small effect on the estimate for d, so that d = 70 to 90 nm for the dry film data in Fig. 3, the worst case example of MAI data analysis. Dry PQ^{2+} films swelled substantially when exposed to solvent vapors. Vapor from pure water caused film swelling of about 125%, while a 1.0 *M* KCl solution gave only about 90% swelling due to its lower vapor pressure. The thickness of films just after immersion in solution equalled their thickness when swollen by the vapor of that solution.

Although undried films dissolved into the deposition solution, dried films were stable in blank electrolyte solution after substantial initial losses, which probably involved diffusion of monomer and short oligomers out of the film. Break-in cycling in blank electrolyte produced reproducible Ψ-Δ plots and narrower, taller, and more symmetrical cyclic voltammograms (CVs). Fitting MAI data for films completely oxidized and reduced during slow CVs gave precise $\tilde{N}$ and d values for films in blank electrolyte solution. Typical data and best fits are plotted in Fig. 4, along with calculated film growth curves for each oxidation state to show how Ψ and Δ depend on d for each state. Results for two films (A and C in Table I) studied over a few days are summarized in Table II. Reduction caused film shrinkage of 0 to 35%, depending upon the age of the film in solution. Freshly deposited films shrank the most and gave the largest $C^*_{PQ^+}$ values. Break-in cycling caused some film loss and increased C^*. Entries in Table II indicate that break-in increased $C^*_{PQ^{2+}}$ by about 20 ± 10%. PQ^{2+} films were significantly more swollen in blank electrolyte solution than during their electrodeposition, as shown by lower $n_{PQ^{2+}}$ and $C^*_{PQ^{2+}}$ values: $n_{PQ^{2+}}$ = 1.46 *vs.* 1.51 and $C^*_{PQ^{2+}}$ = 1.27 *vs.* 1.40 *M*, respectively. $n_{PQ^{2+}}$ for transferred films was almost as low as its value during dissolution of undried films, suggesting that any cross-links formed during film drying did not inhibit swelling.

Treatment of transient Ψ-Δ data requires consideration of the PQ^+ monomer-dimer equilibrium, because of its ef-

Table II. *In situ* film thicknesses, optical constants, and bulk redox concentrations for $PQ^{2+/+}$ films in 1.0 *M* KCl.

Film	Redox state	n [a]	k [a]	d(nm) [b]	Γ (mol/cm²) [c]	C^* (M) [d]	D_{ct} (10^{-9} cm²/s) [e]	Time in soln.
1a	PQ^{2+}	1.457	0	458	4.71×10^{-8}	1.03	—	9 h (virgin)
1b	PQ^{2+}	1.466	0	301	3.79×10^{-8}	1.26	—	1 day
	PQ^+	1.717	0.178	184	3.79×10^{-8}	2.06	—	1 day
1c	PQ^{2+}	1.408	0.008	202	2.18×10^{-8}	1.08	3.0	3 day
	PQ^+	1.519	0.145	152	2.18×10^{-8}	1.43	1.0	3 day
2a	PQ^{2+}	1.456	0	145	1.55×10^{-8}	1.07	—	5 h (virgin)
2b	PQ^{2+}	1.457	0	121	1.55×10^{-8}	1.28	1.6	8 h
	PQ^+	1.508	0.115	106	1.55×10^{-8}	1.46	1.2	8 h

Note: Film 1 was spun cast from EtOH solution and film 2 was electrodeposited; $\tilde{N}_{Pt}$ = 1.86 − 4.15i and 1.80 − 4.60i, respectively.
[a] Estimated error of ±0.008.
[b] Estimated error of ~5%.
[c] From peak areas during slow voltammetric sweeps.
[d] Estimated error of ±0.05 *M*.
[e] From chronocoulometry during large amplitude potential steps, using C^* of initial state.

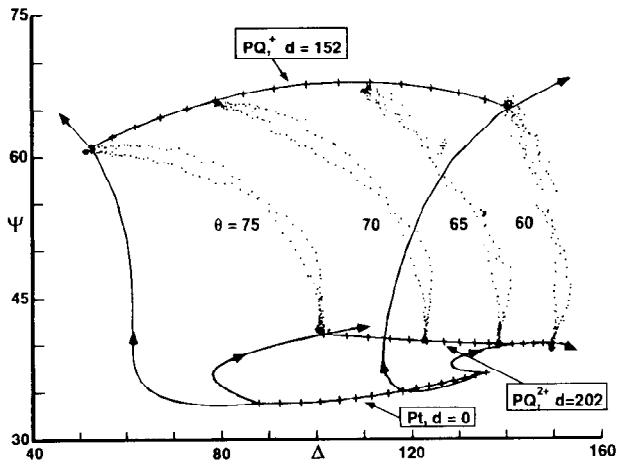

Fig. 4. Ellipsometric data (dots) for ~200 nm film (1c in Table II) during 100 mV/s sweeps (*i.e.*, Fig. 8B): one CV per angle, θ = 60, 65, 70, and 75°; E = 0.0 to −0.785 V; 37 ms/point. Calculated MAI curves (connected + signs) for $\tilde{N}$ and d from best fits of the MAI data for the fully oxidized (PQ^{2+}, d = 202 nm, $\tilde{N}$ = 1.408 − 0.008$\hat{\imath}$) and reduced forms (PQ^{+}, d = 152 nm, $\tilde{N}$ = 1.519 − 0.145$\hat{\imath}$) and for the polished electrode (Pt, d = 0, $\tilde{N}$ = 1.86 − 4.15$\hat{\imath}$) are plotted over the data, along with calculated multiple thickness curves for θ = 60 and 75° only. The arrows indicate the direction of increasing film thickness.

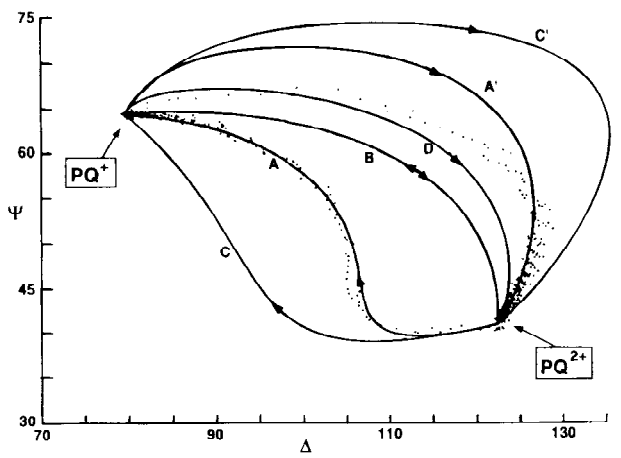

Fig. 6. Ellipsometric data (dots) for film 1c in Table II during multiple 0.5 s potential steps between E = 0.0 and −0.75 V. The bottom set of points from right to left corresponds to reduction and the top set vice versa to oxidation. The solid curves were calculated from conversion profiles for various simulated modes of conversion: (A and A') conversion by diffusional electron transport from/to the electrode; (B) uniform conversions; (C and C') two-layer conversion model; and (D) diffusional charge-transport coupled with dimerization/monomerization reaction channels, that is, Eq. 6 with $k_b = 1.3 \times 10^3\ s^{-1}$, $K = k_f/k_b = 7.7 \times 10^3\ M^{-1}$, and $D_{ct} = 3.0 \times 10^{-9}\ cm^2/s$. $\tilde{N}_{PQ^{2+}}$ = 1.408 − 0.012$\hat{\imath}$, $d_{PQ^{2+}}$ = 201.5 nm, $\tilde{N}_{PQ^{+}}$ = 1.519 − 0.145$\hat{\imath}$, $d_{PQ^{+}}$ = 149.5 nm.

fect on the film optical constants. Dimerization of various viologen radical cations has been studied by electron spin resonance (ESR)[48-50] and UV-vis spectroscopy.[51-57] It is favored in aqueous solutions, at lower temperatures, and at higher viologen radical concentrations[50,55] and can be identified by a blue to violet color shift (absorption λ_{max} = 603 nm to λ_{max} = 550 nm). Intramolecular dimer formation is highly favored in covalently linked systems.[23,38,53,56,57] The positive shift in $E_{1/2}$ for **I** concentrated in a thin film *vs.* in dilute solution can provide an estimate of the dimer formation constant for film-bound PQ^{+} centers (reaction 2). Although theory has been presented for the effects of irreversible dimerization on linear potential-sweep voltammetry of thin-layer systems,[32] we found no treatment of the effects of reversible dimer formation on a nernstian thin-layer system. The expression for this case (see Appendix A) is

$$i/[n^2F^2Vv/4RT] = K^{-1}\theta\{(1 + \theta) - Z\}\{\theta/Z - 1\} \quad [3]$$

where i is the current, $Z = [(1 + \theta)^2 + 8KC^*]^{1/2}$, $\theta = \exp[nF(E - E^{o\prime})/RT]$, E is the electrode potential, $E^{o\prime}$ is the formal potential of the couple in the absence of the dimerization reaction (*i.e.*, in dilute solution), C^* is considered constant (*i.e.*, constant film thickness), $V = A \cdot d$ is the volume of the thin layer, and $K = [(PQ^{+})_2]/[PQ^{+}]^2$ is the dimer formation constant. General analytical expressions for the peak width at half-maximum (FWHM) and peak potential (E_p) could not be found, but in the limiting region of $KC^* > 500$

$$E_p = E^{o\prime} + (RT/2nF) \ln (KC^*) \quad [4]$$

$$E_p = E^{o\prime} + (30/n) \log (KC^*) \quad \text{for } T = 25°C \text{ and } E \text{ in mV} \quad [5]$$

Equation 3 predicts symmetrical mirror image oxidation and reduction peaks, positive of $E^{o\prime}$ when the reduced form of the couple undergoes dimerization and negative of $E^{o\prime}$ when the oxidized form undergoes dimerization. Peaks become taller and narrower (limiting FWHM = 66/n mV for $KC^* > 500$) than for a simple nernstian thin layer system (FWHM = 91/n mV).[4]

Experimental CVs for low sweep rates approached the limiting shape predicted by Eq. 3 (see Fig. 5). Calculated CVs for $KC^* = 1 \times 10^4$ closely matched the size, width, and $E_{1/2}$ of experimental CVs, which were 70 mV wide and about 120 mV positive of $E^{o\prime} = -0.69$ V. ($E^{o\prime}$ was estimated from the average peak potentials, $E_{p,c}$ and $E_{p,a}$, for **I** in dilute solutions.) Experimental peaks were slightly shorter and wider than the limiting theoretical shape, because small oxidation-state gradients probably persisted even at this v. The measured C^* and shift in $E_{1/2}$ provide a good estimate of K: using $C^* = (C^*_{PQ^{2+}} + C^*_{PQ^{+}})/2 = 1.3\ M$ gives $K = 7.7\ (\pm 0.8) \times 10^3\ M^{-1}$, a value an order of magnitude larger than

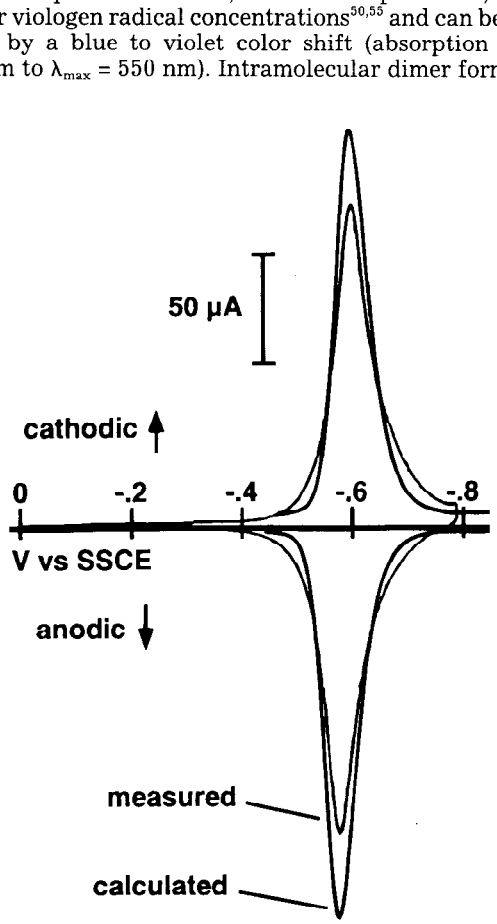

Fig. 5. Comparison of measured CV peaks for a 140 nm film and theoretical peaks from Eq. 3. v = 50 mV/s, C^* = 1.3 M, and $K = 7.7 \times 10^3\ M^{-1}$. Calculated peaks are taller and narrower and were drawn separated by 15 mV to align them with measured peaks for easy comparison of peak shapes.

literature values for methylviologen (MV^{2+}) in solution.[54,55] However, this value is smaller than values for low dimensional systems[58] and is consistent with reports that dimer formation is more favored in covalently linked bis-viologens.[57]

From the expression for the dimer formation constant and its value,[54] one can show that only a few percent of the PQ^+ centers should be monomeric after only a small fraction of the centers are reduced. Absorbance studies have also shown that dimerization of PQ^+ centers is so complete that films behave optically as a two-state system with a negligible concentration of monomeric centers.[38] In this case, k_{PQ^+} should be proportional to the concentration and absorptivity of reduced centers; k is related to the molar absorptivity (ϵ) and concentration of absorbing centers (C) by $4\pi k/\lambda = 2.303\epsilon C$, where λ is wavelength in cm.[59] The k_{PQ^+} and $C^*_{PQ^+}$ values in Table II give an average $\epsilon = 7.6 \pm 1.3 \times 10^3\ M^{-1}\ cm^{-1}$ at 632.8 nm. This value is higher than the value from reported absorbance spectra for PQ^+ films on transparent substrates,[23] $\epsilon = 5.7\ (\pm 0.5) \times 10^3\ M^{-1}\ cm^{-1}$; and for MV^+ in solution,[55] $\epsilon = 4.3\ (\pm 0.3) \times 10^3\ M^{-1}\ cm^{-1}$, a value probably low by about 30% according to Watanabe and Honda.[60]

Potential-step conversion between $PQ^{2+/+}$ states.—By comparing measured data and calculated curves we can use the sensitivity of ellipsometry to oxidation-state gradients to see if the charge transport obeyed the diffusion laws. Ψ-Δ data and calculated curves for film conversion during large amplitude, 0.5 s double-potential steps are given in Fig. 6. Comparing the data to curve B, which represents uniform (zero gradient) conversion of the film between the $\bar{N}$ and d values from MAI analysis, illustrates how concentration gradients cause hysteresis in Ψ-Δ data curves. Calculated curves (C and C') for a two-layer model, where the thickness of the inner layer (final state) grows at the expense of the outer layer (initial state),[25,26] overestimate the sharpness of the conversion boundary and predict more hysteresis than was observed. Note that calculated curves for the case of reduction or oxidation proceeding from the film/solution interface inward to the electrode would appear on the opposite side of curve B from the corresponding data. In fact, traversing curve C' backwards from right to left represents this conversion mode for film reduction and traversing curve C backwards from left to right describes this case for oxidation.

Calculated curve A for effective electron diffusion outward from the electrode via electron hopping between adjacent sites fits the reduction data remarkably well, optically confirming that reduction occurs by a diffusional process. A standard finite-difference method[61,62] was used to simulate charge diffusion (*i.e.*, correlated diffusion of 2+ and + sites) and to generate oxidation state gradients (*i.e.*, fractional concentrations) as a function of fractional time, by dividing the film into at least 18 volume elements stacked normal to the electrode, as described in Appendix B. One Ψ-Δ point was calculated from each concentration profile using the exact equations for a stratified, multilayer system[46] and the $\bar{N}$ and d for each state without any adjustable parameters (see Appendix B). Changes in film thickness were not included in the diffusion simulation but were included in Ψ-Δ calculations. Reduction of the film appeared to be ideal electrochemically as well, and optical and electrochemical conversion finished simultaneously at $t = 370$ ms. Chronocoulometric plots of charge Q *vs.* $t^{1/2}$ were linear at $t \leq 60$ ms (Fig. 7), as expected for semi-infinite diffusion early in the steps. Departure from linearity after 60 ms ($t \approx d^2/2D_{ct}$) was consistent with $D_{ct} = 3.0 \times 10^{-9}$ cm^2/s from the Q-$t^{1/2}$ slope (for $C^* = C^*_{PQ^{2+}} = 1.1\ M$) and with literature values for D_{ct}.[13]

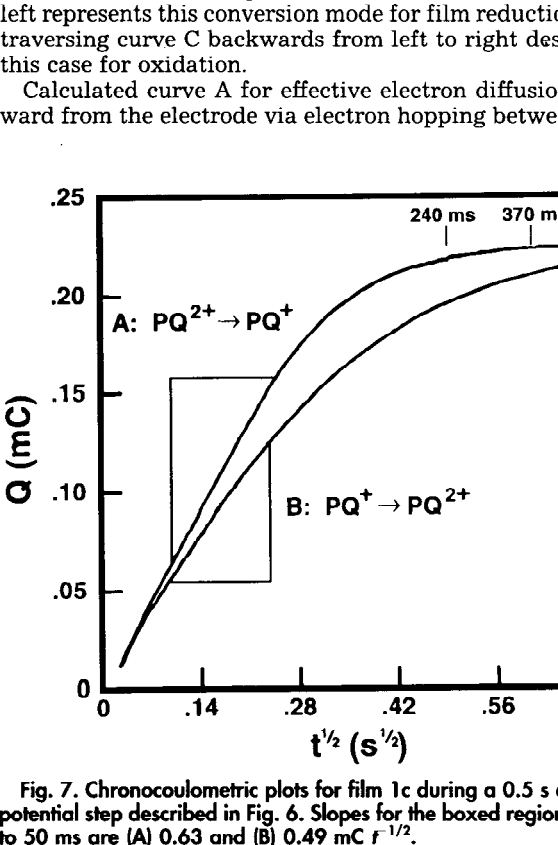

Fig. 7. Chronocoulometric plots for film 1c during a 0.5 s double-potential step described in Fig. 6. Slopes for the boxed region t = 10 to 50 ms are (A) 0.63 and (B) 0.49 mC $t^{-1/2}$.

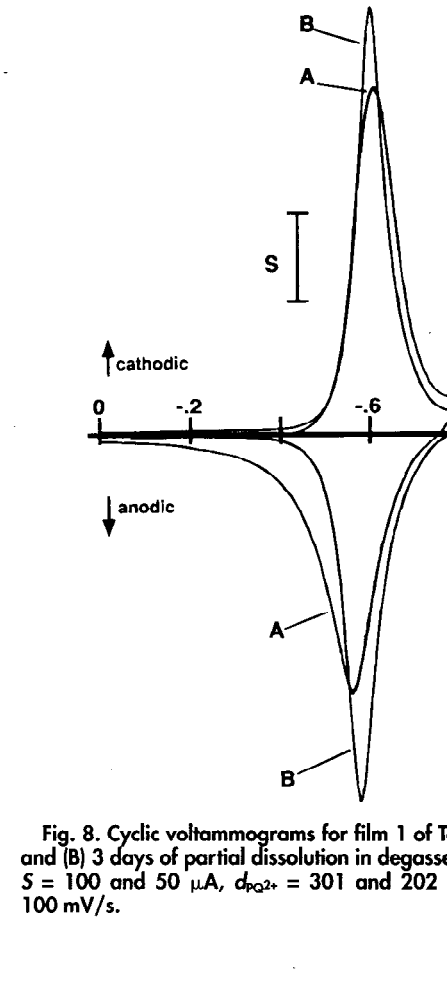

Fig. 8. Cyclic voltammograms for film 1 of Table II after (A) 1 day and (B) 3 days of partial dissolution in degassed 1.0 *M* KCl solution. S = 100 and 50 μA, $d_{PQ^{2+}}$ = 301 and 202 nm, respectively. v = 100 mV/s.

The poor fit of oxidation data by curve A', which was calculated in the same fashion as curve A, shows that oxidation did not conform to a diffusion-controlled process with swelling proportional to the extent of oxidation. The fact that the data fell below the calculated curve early in the conversion suggests that film expansion lagged oxidation at first; note the dependence of Ψ on d for the PQ^+ state as shown in Fig. 4. Q-$t^{1/2}$ plots for oxidation were slightly nonlinear even at small t when semi-infinite conditions should have prevailed (Fig. 7). Least squares fits of 10 ms sections showed that the slope dropped smoothly throughout the conversion. Oxidation was slower than reduction, finishing at t = 500 ms, and the slope of the almost linear portion of the plot (t =10 to 50 ms) gave $D_{ct} = 1.0 \times 10^{-9}$ cm^2/s for $C^* = C^*_{PQ^+} = 1.43\ M$. The nonlinearity and sluggishness

probably represent the impedance to conversion caused by film swelling required for electrolyte influx.

Any preceding reaction or physical process slower than diffusive electron transport can limit the overall rate of film conversion. Examples of rate limiting preceding monomerization reactions and theoretical treatments can be found for potential-sweep[63] and potential-step[64,65] methods. To estimate the importance of the preceeding monomerization reaction to the oxidation rate, its effect was included in simulations by adding terms for the dimerization and monomerization reaction channels to the diffusion equation for PQ^+ using the formulation given by Amatore *et al.*[64]

$$R_{j,(t+\Delta t)} = R_{j,t} + D_M(R_{j+1,t} - 2R_{j,t} + R_{j-1,t}) - 2k_f C^* R_{j,t}^2 \Delta t + 2k_b Z_{j,t} \Delta t \quad [6]$$

$$Z_j = 1/2(1 - O_j - R_j) \quad [7]$$

where k_f and k_b are the forward and backward rate constants for dimer formation and $O_{j,t}$, $R_{j,t}$, and $Z_{j,t}$ are the fractional concentrations of the PQ^{2+}, PQ^+, and $(PQ^+)_2$ in volume element j at time t. Adjusting the value of k_b for $K = k_f/k_b = 7.7 \times 10^3\ M^{-1}$ and $D_{ct} = 3.0 \times 10^{-9}$ cm^2/s produced calculated Ψ-Δ curves lying between the limiting behaviors for this system (*i.e.*, between curves A′ and B in Fig. 6). $k_b = 1.3 \times 10^3\ s^{-1}$ generated curve D and a simulated Q-$t^{1/2}$ slope equal to the observed slope. It was not possible to fit both ends of the data curve, because k_b values that accounted for the early data produced calculated gradients that were smaller than the actual gradients indicated by data late in the oxidation. These results combined with potential-sweep data showing larger gradients for oxidation than reduction suggest that oxidation was not limited by the preceding monomerization reaction.

Potential-sweep conversions.—Ellipsometric data for conversions during cyclic voltammetry also suggest that oxidation was slower as a consequence of forced film expansion. At slow sweep rates, where CVs had equal cathodic and anodic peak currents, equal widths, and completely symmetrical shapes (*e.g.*, Fig. 5), Ψ-Δ plots were free of hysteresis and representative of uniform, gradient-free conversions. At faster sweep rates, the cathodic peak was consistently taller, narrower, and more symmetrical than the anodic peak, especially so for thicker films (Fig. 8). Larger sweep rates and thicker films caused the same effect on peak shapes, indicating that slower charge transport during oxidation caused the oxidation peaks to be smaller and wider. Ellipsometric plots showed a smooth progression from curves without hysteresis at low v to curves representative of large oxidation state gradients at v where current tailing was pronounced. The gradient during oxidation was always slightly larger than during reduction, except at low v where it disappeared as the anodic and cathodic peaks acquired the same size and shape. At a moderate sweep rate, where only small gradients existed and anodic peaks were slightly smaller than cathodic peaks (Fig. 8B), Ψ-Δ plots show that film swelling lagged oxidation at first and became proportional to the extent of oxidation late in the sweep (Fig. 9). Data for early in the oxidative sweep fell below calculated curves for film swelling proportional to degree of oxidation (curves B and A′) and even below data for the end of the reduction. Solid curves were calculated from the concentration profiles of diffusion simulations that used surface concentrations given by the Nernst equation. For the particular film thicknesses and optical constants involved here, low Ψ values early in the sweep indicate that film swelling was not proportional to oxidation. Note that swelling did not begin until after about 60% oxidation, that is, at about the point where the data and calculated curves intersect (see crossed arrows).

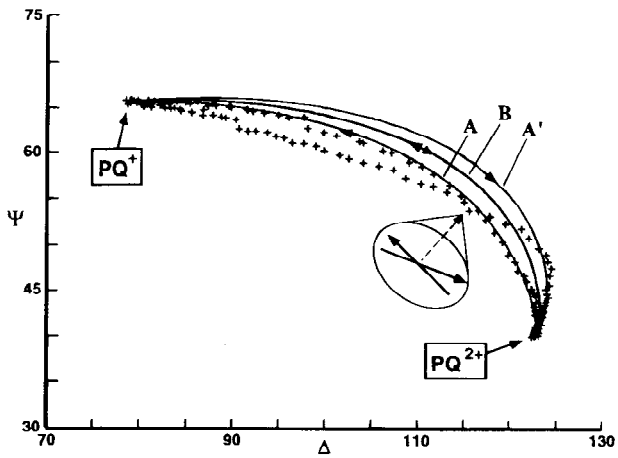

Fig. 9. Ellipsometric data for film 1c during a 100 mV/s CV (CV B in Fig. 8) and calculated curves (A and A′) for simulated diffusional transport during reduction and oxidation, $D_{ct} = 2 \times 10^{-9}$ and $D_{ct} = 1 \times 10^{-9}$ cm^2/s, respectively; and (B) for uniform interconversion, *i.e.*, $D_{ct} \geq 3 \times 10^{-9}$ cm^2/s. See Fig. 4 for optical constants and film thicknesses. $\theta = 70°$.

Discussion

The film-growth data support the proposed model of film formation,[23] where hydrolyzed siloxane centers couple during reductive precipitation of viologen centers to form oligomeric or polymeric siloxanol chains. Monomeric siloxanols are very soluble in aqueous solution, and unreacted oxidized monomers would dissolve instantly. The slow dissolution of undried films indicates that cross-linking and network formation were not significant during film formation, consistent with expected behavior for hydrolysis and oligomerization of trialkoxysilanes[43] and for the early stages of silica formation.[66] Film growth proceeded not because an insoluble network formed but rather as a consequence of slow dissolution and short time spent in the PQ^{2+} state during each cycle.

Solvent swelling of polymers occurs until the internal solvent pressure is balanced against the stress created on cross-links and entanglements that hold the network of chains together.[67] Water swelled PQ^{2+} films to a greater extent than acetonitrile, as expected for a hydrophillic polymer better solvated by a more polar solvent. The refractive index of dried PQ^{2+} films in blank electrolyte solution was about the same as that for undried films undergoing dissolution, indicating that transferred films were highly swollen. Consequently the real part of the refractive index for PQ^{2+} films in aqueous solution was lower than values reported for other electroactive polymer films in their bleached (*i.e.*, almost transparent) state: 1.46 ± 0.04 for PQ^{2+} *vs.* 1.70 for polyphenol (λ = 546 nm);[68,69] 1.63 and 1.50 for polybipyrazine and polyvinylferrocene (λ = 546 nm);[35] 1.8 for polythiophene (λ = 633 nm);[16] and 1.55 to 1.60 for polyaniline (λ = visible region).[26] The low $n_{PQ^{2+}}$ value and hence low density of PQ^{2+} films suggests loosely cross-linked siloxane chains bearing unreacted silanol groups without extensive condensation to give dense siloxane structures, in contrast to the behavior of silicic acid polymers in alkaline solution. It is unlikely that the low $n_{PQ^{2+}}$ value reflects a low intrinsic refractive index or microscopic polarizability for the polymer, because most organic materials have n values near 1.5 and dense homopolymers typically have larger n values than their liquid monomers (by 0.05 to 0.10).[68]

A central question in this study is the effect of film thickness changes on the different charge-transport rates for oxidation and reduction. Ellipsometric results confirmed that film reduction represents a diffusional process, as expected for a well-swollen film with good ionic conductivity. PQ^{2+} films contain a large concentration (about 2.2 M) of counterions and solvent swelling provides ample free volume for ion transport.[70-72] As shown previously,[73] Cl^- is bound more weakly than the other anions investigated, and the largest D_{ct} is found with Cl^- counterion. Furthermore, ΔE_p of CVs was small even for sweep rates up to 50 V/s, and the low glass transition temperatures of polysiloxanes

make them promising candidates as solid polymer electrolytes.[12] Oxidation involved the ingress of counterions into a less swollen, more compact film. The Donnan exclusion principle and permselectivity of the polycationic film dictate that expulsion of Cl^- rather than ingress of K^+ should predominate during reduction. Lower counterion and polymer charge concentrations reduce solvent osmosis. While reduction involved release of internal solvent pressure, film shrinkage, and relaxation of polymer chains to less stretched conformations, oxidation involved the influx of counterions along with solvent molecules. Film shrinkage and reduction occurred concertedly, and mechanical energy (PV work) stored in the stretched film could have assisted reduction of the film.[34] However, oxidation worked against the forces of polymer cohesion, which lowered D_{ct} and CV peak currents for oxidation.

The fact that swelling closely trailed oxidation for conversions at very different rates (*i.e.*, during potential steps and sweeps) suggests that film expansion was caused by ion influx and not merely a secondary process, such as solvent osmosis driven by the energy of dilution. These processes differ in that counterion transport is a field driven process, but solvent osmosis is secondary to ion motion and is not field driven. If counterions were able to enter easily without film expansion, swelling would have been driven only by solvent osmosis, a slower process. Complete swelling of undried films after deposition required several minutes, so swelling by osmosis is slow on the electrochemical time scale. The fact that swelling lagged only shortly behind oxidation, suggests that swelling was forced by counterion migration.

Although the preceding monomerization reaction might have limited the oxidation reaction early in potential steps, when the electrode reaction rate was largest, it could not have been a factor in the cause of different oxidation and reduction charge transport rates observed at slower conversion rates, *e.g.*, during CV sweeps. The similar magnitude of D_{ct} for oxidation and reduction indicates the rate of monomerization was at least comparable to the electron diffusion rate. Any monomerization rate consistent with oxidation rates for potential steps would be too large to limit rates during slow sweeps. Furthermore, any limitation of electrode kinetics would reduce gradients in the film, but in fact larger gradients were observed ellipsometrically for oxidation than reduction during CVs. A more reasonable explanation of the smaller anodic currents is that the impediment of forced film swelling lowered the charge-transport rate.

Summary

This study shows that laws of diffusion are obeyed during reduction of PQ^{2+} films, but oxidation of PQ^+ films is impeded by slow film swelling necessary for influx of counterions. Film shrinkage occurs simultaneously with reduction, but film swelling lags behind oxidation initially and then becomes proportional to the extent of oxidation. Cross-linking in electroprecipitated films of compound **I** is not significant until films are dried. Films in the 2+ state are highly swollen by aqueous solution ($C^* = 1.2 \pm 0.1\ M$) with densities close to that for uncross-linked films undergoing dissolution, and reduced films are denser ($C^* > 1.4 \pm 0.1\ M$) with PQ^+ centers extensively dimerized. The theory presented here adequately predicts the potential shifts and peak shapes for thin layer, linear sweep voltammetry of a redox couple in equilibrium with its dimer.

Acknowledgment

The support of this research by the National Science Foundation (CHE 9214480) is gratefully acknowledged.

Manuscript submitted Jan. 9, 1995; revised manuscript received July 14, 1995.

The University of Texas at Austin assisted in meeting the publication costs of this article.

APPENDIX A

Derivation of Equations for Nernstian Electron Transfer with Fast Reversible Dimerization of Product under Thin Layer Conditions.

Consider the following reaction scheme

$$O + ne \leftrightharpoons R \text{ (with formal potential } E^{\circ\prime}) \qquad [A\text{-}1]$$

$$2R \leftrightharpoons D \text{ (with equilibrium constant } K) \qquad [A\text{-}2]$$

The current is proportional to the rate of electrolysis of O as follows

$$i = -nF\left[\frac{dN_O}{dt}\right] = nF\left[\frac{dN_O}{dE}\right]v \qquad [A\text{-}3]$$

where N_O is the total number of moles of O in the film and $v = -(dE/dt)$ is the sweep rate. Under conditions where concentrations remain uniform (*i.e.*, at slow sweep rates), the concentration of O is

$$C_O = \frac{N_O}{V} \qquad [A\text{-}4]$$

where V is the volume of the film. Substituting for N_O gives

$$\frac{i}{nFV} = \left[\frac{dC_O}{dE}\right]v \qquad [A\text{-}5]$$

Conservation of mass gives

$$C^* = C_O + C_R + 2C_D \qquad [A\text{-}6]$$

where C^* is the total concentration of redox centers and C_O, C_R, and C_D are the concentrations of O, R, and D, respectively. For nernstian kinetics

$$\frac{C_O}{C_R} = \exp\left[\left(\frac{nF}{RT}\right)(E - E^{\circ})\right] \qquad [A\text{-}7]$$

Let $\theta = C_O/C_R$ and $K = C_D/C_R^2$. Substitution into Eq. A-6 gives

$$\theta C_R + C_R + 2KC_R^2 = C^* \qquad [A\text{-}8]$$

Solving this quadratic equation for C_R gives

$$C_R = \frac{-(1+\theta) \pm \sqrt[2]{(1+\theta) + 8KC^*}}{4K} \qquad [A\text{-}9]$$

or

$$C_R = \frac{Z - (1+\theta)}{4K} \qquad [A\text{-}10]$$

for

$$Z = [(1+\theta)^2 + 8KC^*]^{1/2} \qquad [A\text{-}11]$$

Differentiating $C_O = \theta C_R$ gives

$$\frac{dC_O}{dE} = \theta\left(\frac{dC_R}{dE}\right) + C_R\left(\frac{d\theta}{dE}\right) \qquad [A\text{-}12]$$

Differentiating Eq. A-7, A-10, and A-11 gives

$$\left(\frac{d\theta}{dE}\right) = nf\theta \qquad \text{for } f = F/RT \qquad [A\text{-}13]$$

$$\frac{dC_R}{dE} = \frac{1}{4K}\left[\frac{dZ}{dE} - \frac{d\theta}{dE}\right] \qquad [A\text{-}14]$$

and

$$\frac{dZ}{dE} = Z^{-1}(1+\theta)\left[\frac{d\theta}{dE}\right] \qquad [A\text{-}15]$$

Substituting Eq. A-13 and A-15 into Eq. A-14 gives

$$\frac{dC_R}{dE} = \frac{nf\theta}{4K}[Z^{-1}(1+\theta) - 1] \qquad [A\text{-}16]$$

Substituting Eq. A-10, A-13, and A-16 into Eq. A-12 and rearranging gives

$$\frac{dC_O}{dE} = \frac{nf\theta}{4K}[(1+\theta) - Z][\theta/Z - 1] \qquad [A\text{-}17]$$

which upon substitution into Eq. A-5 gives the current per unit volume of film at total concentration C^*

$$\frac{i}{nFV} = \frac{nF\theta v}{4RTK}[(1+\theta) - Z][\theta/Z - 1] \qquad [A\text{-}18]$$

APPENDIX B

Finite-Difference Simulation of Diffusion in a Thin Layer

The layer was divided into volume elements of equal thickness Δx stacked normal to the electrode and indexed by j. Fractional concentrations for each oxidation state ($O_j = [PQ^{2+}]_j/C^*$ and $R_j = [PQ^+]_j/C^*$) were calculated for time $t + \Delta t$ from the fractional concentrations at time t and the flux between adjacent volume elements during interval Δt, as follows

$$O_{j,(t+\Delta t)} = O_{j,t} + D_M(O_{j+1,t} - 2O_{j,t} + O_{j-1,t}) \quad O_{j,(t=0)} = 1.0 \quad [B\text{-}1]$$

$$R_{j,(t+\Delta t)} = 1 - O_{j,(t+\Delta t)} \quad R_{j,(t=0)} = 0 \quad [B\text{-}2]$$

where $D_M = D_{ct}\Delta t/(\Delta x)^2$. $D_M = 0.45$ was used to ensure stable simulations, which in effect kept Δx larger than the diffusion length for each iteration, $(2 \cdot \Delta t \cdot D_{ct})^{1/2}$. The number of volume elements, $j_{max} = d/\Delta x$, was made large enough to ensure that fractional concentrations produced a smooth diffusion gradient in plots of $O_{j,t}$ *vs.* j for both early and late times. About 30 layers were necessary to obtain very smooth concentration profiles, but as few as 18 layers could be used without noticeably affecting the Ψ-Δ conversion curve. Complete conversion of the layer occurred when the number of iterations (i_{max}) was excessively large compared to j_{max}, that is, $i_{max} = 10 \cdot j_{max}$. Note that D_{ct} determines the rate and completion time for diffusion-controlled conversion but not the shape of the concentration profile for a particular degree of conversion.

When two states mix isotropically on a molecular scale, the Lorentz-Lorenz effective medium expression should hold,[74] and one can calculate the $\tilde{N}$ and d of the jth layer (n_j, k_j, and d_j) from the $\tilde{N}$ and d for each state and the fractional concentrations. Although a simple average is inconsistent with rigorous effective medium theory, calculations showed that a simple, weighted average was in error by only about 2% compared to the Lorentz-Lorenz expression, because the difference in n for the two states was small.[45b] The optical constants of each layer were calculated as simple averages to reduce computation time, that is

$$n_j = f_{j,a}n_a + f_{j,b}n_b$$

$$k_j = f_{j,a}k_a + f_{j,b}k_b$$

$$d_j = f_{j,a}d_a + f_{j,b}d_b$$

$$f_{j,a} = 1 - f_{j,b} = C_{j,a}/C_j^*$$

where a and b represent the 2+ and 1+ states of the film, and $f_{j,a}$ and $f_{j,b}$ are the fractional concentrations of each state. Describing the 1+ state as PQ^+ or $(PQ^+)_2$ is not important for the optical treatment of a two-state system.

REFERENCES

1. (a) G. Inzelt, in *Electroanalytical Chemistry,* Vol. 18, A. J. Bard, Editor, p. 1, Marcel Dekker, Inc., New York (1993); (b) I. Rubinstein, in *Applied Polymer Analysis and Characterization,* J. Mitchell, Jr., Editor, p. 233, Hanser, New York (1991); (c) L. R. Faulkner, *Electrochim. Acta,* **34,** 1699 (1989).
2. (a) R. W. Murray, in *Annual Review of Materials Science,* Vol. 14, R. A. Huggins, J. A. Giordmaine, and J. B. Wachtman, Jr., Editors, p. 145, Annual Reviews, Palo Alto, CA (1984); (b) R. W. Murray in *Electroanalytical Chemistry,* Vol. 13, A. J. Bard, Editor, p. 191, Marcel Dekker, Inc., New York (1984).
3. (a) F. B. Kaufman and E. M. Engler, *J. Am. Chem. Soc.,* **101,** 549 (1979); (b) F. B. Kaufman, A. H. Schroeder, E. M. Engler, S. R. Krammer, and J. Q. Chambers,*ibid.,* **102,** 483 (1980).
4. (a) E. Laviron, *J. Electroanal. Chem.,* **112,** 1 (1980); (b) C. P. Andrieux and J. M. Savéant, *ibid.,* **111,** 377 (1980); (c) H. S. White, J. Leddy, and A. J. Bard, *J. Am. Chem. Soc.,* **104,** 4811 (1982).
5. A. H. Schroeder and F. B. Kaufman, *J. Electroanal. Chem.,* **113,** 209 (1980).
6. A. H. Schroeder, F. B. Kaufman, V. Patel, and E. M. Engler, *ibid.,* **113,** 193 (1980).
7. P. Daum and R. W. Murray, *ibid.,* **103,** 289 (1979).
8. M. Majda and L. R. Faulkner, *ibid.,* **169,** 77 (1984).
9. (a) J. C. Jernigan, C. E. D. Chidsey, and R. W. Murray, *J. Am. Chem. Soc.,* **107,** 2824 (1985); (b) J. C. Jernigan and R. W. Murray, *ibid.,* **109,** 1738 (1987).
10. P. Daum, J. R. Lenhard, D. Rolison, and R. W. Murray, *ibid.,* **102,** 4649 (1980).
11. N. Oyama and F. C. Anson, *This Journal,* **127,** 640 (1980).
12. J. R. Owen, in *Electrochemical Science and Technology of Polymers,* Vol. 1, R. G. Linford, Editor, Chap. 3, Elsevier Applied Science, Essex, England (1987).
13. T. J. Lewis, H. S. White, and M. S. Wrighton, *J. Am. Chem. Soc.,* **106,** 6947 (1984).
14. K. Shigehara, N. Oyama, and F. C. Anson, *ibid.,* **103,** 2552 (1981).
15. J. Leddy and A. J. Bard, *J. Electroanal. Chem.,* **153,** 223-242 (1983).
16. A. Hamnett and A. R. Hillman, *ibid.,* **233,** 125 (1987); A. Hamnett and A. R. Hillman, *Ber. Bunsenges. Phys. Chem.,* **91,** 329 (1987).
17. F. C. Anson, T. Ohsaka, and J. M. Savéant, *J. Phys. Chem.,* **87,** 640 (1983).
18. J. Q. Chambers, F. B. Kaufman, and K. H. Nichols, *J. Electroanal. Chem.,* **142,** 277 (1982).
19. W. J. Albery, M. G. Boutelle, P. J. Colby, and A. R. Hillman, *ibid.,* **133,** 135 (1982).
20. G. Inzelt, J. Bacskai, J. Q. Chambers, and R. W. Day, *ibid.,* **201,** 301-314 (1986).
21. J. M. Savéant, *ibid.,* **201,** 211 (1986).
22. F. Helfferich, *Ion Exchange,* p. 267, McGraw-Hill, New York (1962).
23. D. C. Bookbinder and M. S. Wrighton, *This Journal,* **130,** 1080 (1983).
24. (a) D. C. Bookbinder, N. S. Lewis, and M. S. Wrighton, *J. Am. Chem. Soc.,* **103,** 7656 (1981); (b) R. N. Dominey, N. S. Lewis, J. A. Bruce, D. C. Bookbinder, and M. S. Wrighton, *ibid.,* **104,** 467 (1982).
25. (a) M. A. Hopper and J. L. Ord, *This Journal,* **120,** 183 (1973); (b) J. C. Clayton and D. J. DeSmet, *ibid.,* **123,** 174 (1976).
26. S. Gottesfeld, A. Redondo, and S. W. Feldberg, *ibid.,* **134,** 271 (1987).
27. C. Lee, J. Kwak, and A. J. Bard, *ibid.,* **136,** 3720 (1989).
28. F. Chao and M. Costa, *Synth. Met.,* **39,** 97 (1990).
29. C. Lee, J. Kwak, L. J. Kepley, and A. J. Bard, *J. Electroanal. Chem.,* **282,** 239 (1990).
30. Y. Morishima, I. Akihara, H. S. Lim, and S. Nozakura, *Macromolecules,* **20,** 978 (1987).
31. (a) G. Inzelt, R. W. Day, J. F. Kinstle, and J. Q. Chambers, *J. Phys. Chem.,* **87,** 4592 (1983); (b) G. Inzelt, R. W. Day, J. F. Kinstle, and J. Q. Chambers, *J. Electroanal. Chem.,* **161,** 147 (1984).
32. E. Laviron, *This Journal,* **39,** 1 (1972).
33. P. Daum and R. W. Murray, *J. Phys. Chem.,* **85,** 389 (1981).
34. C. M. Carlin, L. J. Kepley, and A. J. Bard, *This Journal,* **132,** 353 (1985).
35. E. F. Bowden, M. F. Dautartas, and J. F. Evans, *J. Electroanal. Chem.,* **219,** 49 (1987).
36. M. Majda and L. R. Faulkner, *ibid.,***169,** 97 (1984).
37. (a) C. E. D. Chidsey, B. J. Feldman, C. Lundgren, and R. W. Murray, *Anal. Chem.,* **58,** 601 (1986); (b) X. Chen, P. He, and L. R. Faulkner, *J. Electroanal. Chem.,* **222,** 223 (1987).
38. J. G. Gaudiello, P. K. Ghosh, and A. J. Bard, *J. Am. Chem. Soc.,* **107,** 3027 (1985).
39. S. V. Pihlajamaki and J. J. Kankare, *J. Electroanal. Chem.,* **170,** 195 (1984).
40. M. A. Barrett and R. Parsons, *Symp. Faraday Soc.,* **4,** 72 (1970).
41. Y-C. Chiu and M. A. Genshaw, *J. Phys. Chem.,* **73,** 3571 (1969).
42. P. Drude, *The Theory of Optics,* p. 366, Dover Publications, New York (1959).
43. E. P. Plueddemann, *Silane Coupling Agents,* Chap. 3, Plenum, New York (1982).
44. K. W. Willman and R. W. Murray, *J. Electroanal. Chem.,* **133,** 211 (1982).
45. (a) L. J. Kepley and A. J. Bard, *Anal. Chem.,* **60,** 1459 (1988); (b) L. J. Kepley, Ph.D. Thesis, University of Texas, Austin, TX (1990).
46. (a) R. M. A. Azzam and N. M. Bashara, *Ellipsometry and Polarized Light,* Chap. 4, North-Holland, Amsterdam (1977); (b) D. den Engelsen, *J. Opt. Soc. Am.,* **61,** 1460 (1971).
47. L. Bohn, in *Polymer Handbook,* 2nd ed., J. Brandrup and E. H. Immergut, Editors, p. III-241, Wiley, New York (1975).
48. A. L. Rieger and P. H. Rieger, *J. Phys. Chem.,* **88,** 5945 (1984).

49. A. G. Evans, J. C. Evans, and M. W. Baker, *J. Chem. Soc., Perkin 2*, 1787 (1977).
50. V. F. Ivanov and A. D. Grishnia, *Izv. Akad. Nauk SSSR, Ser. Khim.*, **8**, 1873 (1977).
51. L. A. Summers, *The Bipyridinium Herbicides*, p. 97, Academic Press Inc., New York (1980).
52. For a review of the viologens, see, C. L. Bird and A. T. Kuhn, *Chem. Soc. Rev.*, **10**, 49 (1981).
53. H. Kamogawa, H. Mizuno, Y. Todo, and M. Nanasawa, *J. Polym. Sci. Polym. Chem. Ed.*, **17**, 3149 (1979).
54. R. N. F. Thorneley, *Biochim. Biophys. Acta*, **333**, 487, (1974).
55. E. M. Kosower and J. L. Cotter, *J. Am. Chem. Soc.*, **86**, 5524 (1964).
56. H. Sato and T. Tamamura, *J. Appl. Polym. Sci.*, **24**, 2075 (1979).
57. P. Neta , M.-C. Richoux, and A. Harriman, *J. Chem. Soc. Faraday Trans. 2*, **81**, 1427 (1985).
58. (a) A. J. Frank, M. Grätzel, and J. J. Kozak, *J. Am. Chem. Soc.*, **98**, 3317 (1976); (b) J. J. Ramsden and M. Grätzel, *Chem. Phys. Lett.*, **132**, 269 (1986); (c) J. Prasad and R. Kopelman, *J. Phys. Chem.*, **91**, 265 (1987).
59. (a) A. R. Hillman, E. F. Mallen, and A. Hamnett, *J. Electroanal. Chem.*, **244**, 353 (1988); (b) S. Gottesfeld, in *Electroanalytical Chemistry*, Vol. 15, A. J. Bard, Editor, p. 143, Marcel Dekker, Inc., New York (1989).
60. T. Watanabe and K. Honda, *J. Phys. Chem.*, **86**, 2617 (1982).
61. A. J. Bard and L. R. Faulkner, *Electrochemical Methods*, Appendix B, Wiley, New York (1980).
62. S. W. Feldberg, in *Electroanalytical Chemistry*, Vol. 3, A. J. Bard, Editor, p. 199, Marcel Dekker, Inc., New York (1969).
63. J. M. Savéant and E. Vianello, *Electrochim. Acta.*, **12**, 629 (1967); *ibid.*, 1545-1561.
64. C. Amatore, D. Garreau, M. Hammi. J. Pinson, and J. M. Savéant, *This Journal*, **184**, 1 (1985).
65. (a) M. L. Olmstead and R. S. Nicholson, *Anal. Chem.*, **41**, 851 (1969); (b) B. M. Bezilla and J. T. Maloy, *This Journal*, **126**, 579 (1979).
66. R. K. Iler, *Surf. Colloid Sci.*, **6**, 1 (1973).
67. L. Rebenfeld, P. J. Makarewicz, H.-D. Weigmann, and G. L. Wilkes, *J. Macromol. Sci., Chem.*, **C15**, 297 (1976).
68. M. Babai and S. Gottesfeld, *Surf. Sci.*, **96**, 461 (1980).
69. J. F. Wall, J. C. Brumfield, R. W. Murray, and E. A. Irene, *This Journal*, **141**, 306 (1994).
70. T. G. Fox and P. J. Flory, *J. Polym. Sci.*, **14**, 315 (1954).
71. M. L. Williams, R. F. Landel, and J. D. Ferry, *J. Am. Chem. Soc.*, **77**, 3701 (1955).
72. M. H. Cohen and D. Turnbull, *J. Chem. Phys.*, **31**, 1164 (1959).
73. J. A. Bruce and M. S. Wrighton, *J. Am. Chem. Soc.*, **104**, 74 (1982).
74. D. E. Aspnes, *Thin Solid Films*, **89**, 249 (1982).

Electrochemical Methoxylation of Porous Silicon Surface

M. Warntjes, C. Vieillard, F. Ozanam, and J.-N. Chazalviel*

Laboratoire de Physique de la Matière Condensée,[a] CNRS-École Polytechnique, 91128 Palaiseau, France

ABSTRACT

An electrochemical process aiming at the grafting of methoxy groups on the hydrogenated porous silicon surface at room temperature has been designed. This takes place through partial anodic dissolution of porous silicon in anhydrous methanol. A dissolution mechanism is proposed by analogy with that of the anodic dissolution of silicon in aqueous fluoride media. The methoxylated surface exhibits improved optical characteristics (increased photoluminescence efficiency, blue shift of the emission), similar to porous silicon anodically oxidized in a nonfluoride aqueous electrolyte. Its stability against aging is also improved as compared to that of the hydrogenated surface, but without reaching the stability of anodically oxidized porous silicon. This residual sensitivity to aging is ascribed to the nonnegligible amount of SiH species which remains on the methoxylated surface upon the modification process.

Introduction

Porous silicon is usually formed in a concentrated HF-based electrolyte, by anodic dissolution of a silicon crystal. It has been known for several years that immediately after emersion from this electrolyte as well as during the dissolution reaction, the porous silicon surface is covered by SiH bonds.[1-3] The role of the surface has been invoked either as a part of the luminescence recombination scheme in porous silicon, or as a key factor for surface passivation in order to prevent nonradiative recombination and thus reach a good luminescence efficiency.[4-6] The hydride-passivated surface obtained after porous silicon formation, and also on a planar silicon crystal after an HF dip, results in good electronic properties (*e.g.*, low surface recombination velocity[7]). On a single-crystal silicon surface, the hydride passivated surface is known to exhibit a fair stability against oxidation, at least on a time scale of a few hours.[8] In contrast, the porous silicon surface is much more prone to oxidation, and, especially for the high porosity samples, the infrared spectra exhibit traces of such an oxidation after a few tens of minutes in air.

Chemical stabilization of the material and conservation (or enhancement) of the luminescence efficiency are two current challenges faced in the development of porous-silicon-based light emitters. As is known, good chemical stabilization is obtained upon oxidizing the porous silicon surface, either thermally or by anodic oxidation. But this does not appear as a promising route for device application, because this impedes electrical carrier injection. On the other hand, on flat silicon crystals, methoxylation of the surface has been reported as a key factor in order to account for the long-term stability and the low interfacial recombination characteristics in methanol-based photoelectrochemical cells.[9] Similar modification of the porous silicon surface then appears highly attractive since it might provide a much more stable surface which could be used as a tool, either for device applications or for the test of fundamental models aiming at explaining the mechanisms involved in the luminescence of porous silicon.

In the present work, we report on an electrochemical process which allows for the partial substitution of the hydride coverage of the porous silicon surface by methoxy groups. Such electrochemical treatments appear very attractive for grafting organic species unable to react chemically with the porous silicon surface.[10] The experimental procedure of the modification is described first, then the characterization of the modified samples by infrared and photoluminescence spectroscopies are reported. Finally, the results and their practical consequences are discussed.

* Electrochemical Society Active Member.
[a] Unité de Recherche 1254 Associée au Centre National de la Recherche Scientifique.